ORIGINAL ARTICLE

Isoform-specific determinants in the HP1 binding to histone 3: insights from molecular simulations

Matias R. Machado · Pablo D. Dans · Sergio Pantano

Abstract Despite the significant improvements in anti HIV-1 treatment, AIDS remains a lifelong disease due to the impossibility to eradicate the viral reservoir established upon integration of the viral genome. Controlling the epigenetic block imposed by the host cell machinery to the viral transcription may represent a therapeutic alternative to purge the viral reservoir, offering a way to eradicate the infection. Heterochromatin protein 1 (HP1) has been reported to actively participate in the silencing of HIV-1 integrated genome by binding to histone 3 (H3) tail. This interaction is mediated by the Chromodomain of HP1. Nevertheless, the structural features that determine its binding to H3 tail upon post-transductional modifications, such as methylation and phosphorylation as well as isoform-specific effects have not yet been described. We have undertaken the systematic simulation of the Chromodomains of the isoforms beta and gamma of HP1 in complex with the H3 tail methylated at Lys9 in presence/absence of phosphorylation at Ser10. Our results pinpoint isoform-specific electrostatic interactions as important determinants for the stability of the complexes. Characterization of intermolecular contacts between HP1 variants and H3 furnishes new insights on isoform-specific recognition and the effect of phosphorylation.

Keywords Epigenetics · HIV-1 · Transcription · Phosphorylation · Methylation

M. R. Machado · P. D. Dans · S. Pantano (✉)
Institut Pasteur of Montevideo, Mataojo 2020,
11400 Montevideo, Uruguay
e-mail: spantano@pasteur.edu.uy

S. Pantano
IMASL, CONICET, National University of San Luis,
Ejercito de los Andes 950, CP 4700, San Luis, Argentina

Introduction

HIV-1 infection can be effectively controlled by highly active anti-retroviral therapy, with a clear improvement in the life quality of the infected individuals (Clavel and Hance 2004; Martinez-Cajas and Wainberg 2008). However, current therapies cannot cure HIV-1 disease and compliance failures cause rebound of viremia, favouring the evolution of escape variants that are resistant to current drugs (McKinnon et al. 2009). Hence, there is still a need for drugs directed towards different targets, other than those addressed by current therapies, and for treatments that go in the direction of curing the disease by eradicating the infection. Therapeutic targeting of viral post-integration latency is a major goal to attempt HIV-1 eradication (Pierson et al. 2000).

The repression imposed by chromatin is an important factor for maintenance of viral reservoirs and several strategies that selectively activate quiescent proviral genomes with relatively limited effects on the host cell have been proposed (Ylisastigui et al. 2004; Lehrman et al. 2005). In that sense, the understanding of the molecular mechanisms involved in the silencing/repression of the integrated retroviral genome remains largely unknown. It has been hypothesized that heterochromatin machinery and repressive histone marks may play a determining role in chromatin-mediated HIV-1 transcriptional silencing (Marban et al. 2007). It is widely known that histone methylation is involved in heterochromatin assembly and gene silencing (Grewal and Moazed 2003). In particular, Heterochromatin protein 1 (HP1) specifically recognizes histone 3 (H3) methylated at Lys9 (Bannister et al. 2001; Jacobs et al. 2001; Lachner et al. 2001). A consequence of HP1 recruitment is the establishment of a chromatin repressive state that leads to gene silencing (Grewal and

🕲 Springer

Moazed 2003; Maison and Almouzni 2004). In humans there are three isoforms of HP1 that differ in its nuclear localization (Maison and Almouzni 2004). While HP1 α and β are mainly concentrated at pericentric heterochromatin, HP1γ also localizes to euchromatic sites (Minc et al. 2000; Nielsen et al. 2001). It has been reported that in absence of stimulation, HP1β is present on the HIV-1 promoter together with the non-processive RNAPII and functions as a negative regulator. However, HP1β bound to H3 methylated at Lys9 may be released concurrent with H3 phospho-acetylation, and replaced by HP1γ (Mateescu et al. 2008). This isoform localizes to the HIV-1 promoter but also inside the coding region, together with the processive RNAPII (Nielsen et al. 2001). An independent line of evidence established that HIV-1 reactivation could be achieved after RNA interference against HP1γ in different cellular models, suggesting that targeting only the HP1γ isoform can be sufficient to achieve HIV-1 derepression (du Chéné et al. 2007). Therefore, derepression of chromatin at the HIV-1 integration site by modulating the interaction between H3 trimethylated at Lys9 (H3K9Me3) and HP1 may represent a target for drugs aiming at reactivating the virus from post-integrative latency.

Several reports suggest that the epigenetic mark to release H3K9Me3-mediated repression is the phosphorylation of H3 at Ser10 (H3S10p) (Fischle et al. 2005; Hirota et al. 2005; Johansen and Johansen 2006). However, some controversy remains as it has been proposed that this post-transductional modification can be tolerated by the HP1–H3K9Me3 complex (Mateescu et al. 2004). In addition to H3S10p, acetylation of H3 at Lys14 has also been proposed to abrogate the protein–protein interaction (Mateescu et al. 2004).

HP1 binds to H3K9Me3 through a very conserved folding module called Chromodomain (from CHROmatin MOdifier). This domain is formed by nearly 60 residues folded in a three-strand β-roll ended by a C-terminal α-helix (Fig. 1a, b). This architecture gives place to a binding site where an extended peptide binds forming an anti-parallel β-sheet between strand β1 and residues of the β3-α1 loop, which in absence of the ligand remain unstructured (Ball et al. 1997). The binding pocket contains a critical Triptophan and two Tryrosine/Phenilalanines that coordinate the binding of a three or dimethylated Lysine via a triple cation-π interaction. Affinity is further strengthened by the presence of a highly conserved acidic residue, which confers to the trimethyl lysine unique recognition characteristics (Jacobs and Khorasanizadeh 2002).

The high similarity between HP1 isoforms (Fig. 1a) suggests that subtle differences in the binding domain may determine differential interactions with H3K9Me3. Only a few experimental structures of HP1 Chromodomain in complex with a methylated histone tail are available (Jacobs

and Khorasanizadeh 2002; Nielsen et al. 2002), while no structural information is currently known for the Ser10 phosphorylated form of the adduct, nor for the γ isoform.

In this contribution we aim to provide a comparative view into the structural determinants that rule the complexes between H3K9Me3 and isoforms β and γ of HP1, which are involved in HIV-1 promoter transcription/silencing (du Chéné et al. 2007; Mateescu et al. 2008). Moreover, in an effort to provide new insights onto the effect of phosphorylation at Ser10 we constructed structural models of the doubly modified complex (HP1–H3K9Me3S10p). Molecular dynamics (MD) simulations were used to relax the models and evaluate its interactions and stability upon temperature effects.

Our results point to a higher stability of the complex with HP1β compared to that with HP1γ. Ligand detachment upon phosphorylation at Ser10 was not observed (perhaps due to limited sampling time). Modification of this residue seems to be more tolerated in the γ isoform owing to a reduced electrostatic repulsion. This study highlights the influence of the interactions between the N-terminal of the Chromodomain and basic residues at both sides of the trimethylation site. These contacts are isoform specific and could be exploited to increase the selectivity of rationally designed compounds with potential anti HIV-1 activity.

Methods

Molecular systems

We used as template the structure of the mouse HP1β Chromodomain (considered as the receptor) bound to a peptide from H3 dimethylated at lysine 9 (considered as the ligand) (PDB entry 1GUW; Nielsen et al. 2002). It is expected to be identical to the human counterpart (100% of identity within the region used in this work comprising the Chromodomain, i.e. residues 15 to 72 in mouse and human). It is worth to notice that Lys9 in this structure is dimethylated instead of trimethylated. Nevertheless, structural comparison between di- and trimethylated H3 peptides bound to the Drosophila HP1 Chromodomain shows that the only minor differences regarding the coordination of a water molecule by the dimethylammonium moiety (Jacobs and Khorasanizadeh 2002). Therefore, no changes were introduced in the receptor scaffold. Dimethylation present at lysine 4 of the ligand peptide was removed.

Starting from the NMR structure (Nielsen et al. 2002), five systems were built

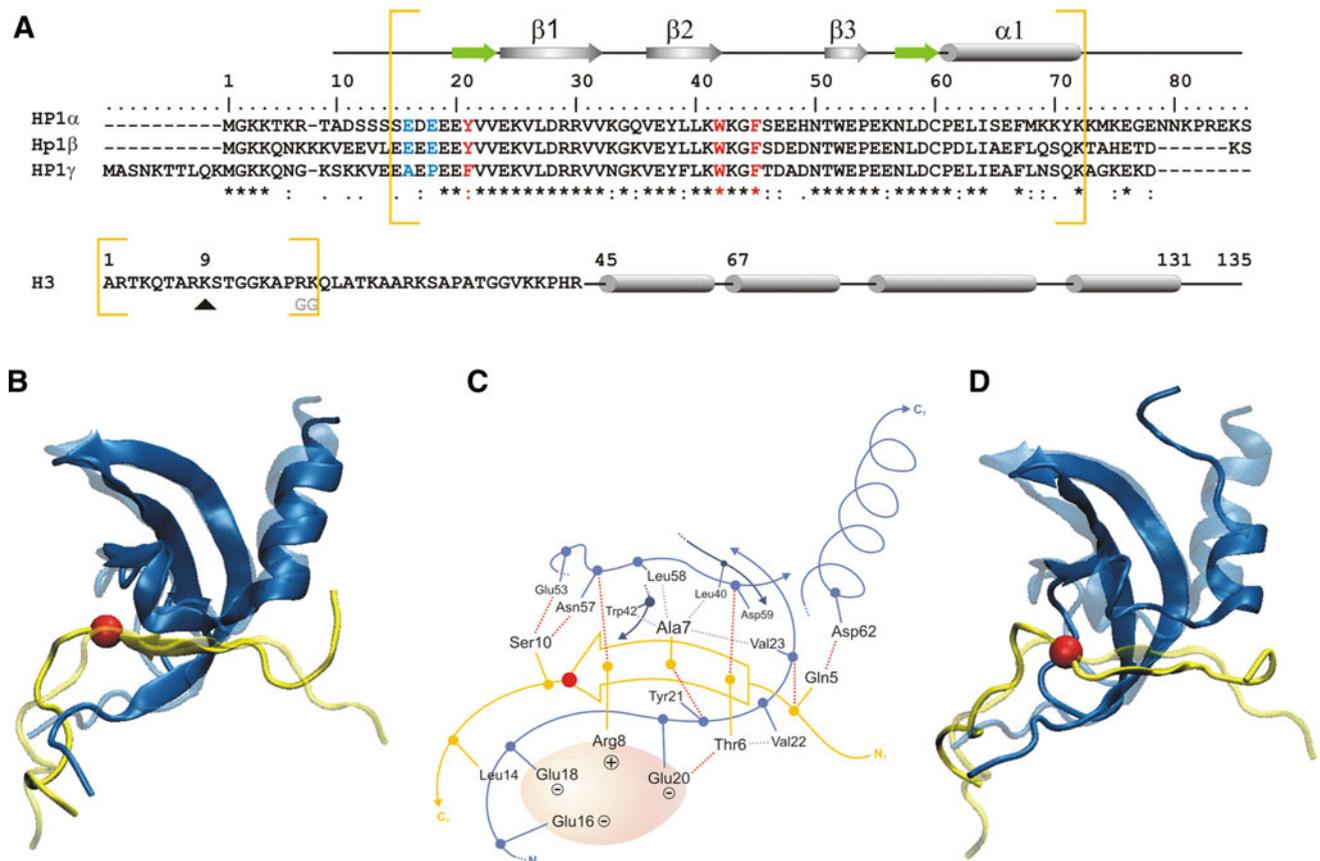(i) A complex of the human HP1β bound to the N-terminal 18-mer of H3 trimethylated at Lys9 (H3K9Me3). This

Fig. 1 Molecular systems and interactions. **a** *Top* Sequence alignment of the N-terminal segment of the three human isoforms of HP1. The secondary structure is indicated on the top of the alignment. *Green arrows* represent protein segments which structure approaches to a β-strand upon H3 binding. *Squared brackets* indicate the region comprising the structure of the Chromodomain used in this work. *Red* residues are conserved amino acids constituting the aromatic cage for cation-π interaction. *Blue* residues depict sequence changes in β and γ isoforms at the N-terminal region of the model. Numbering corresponds to the beta isoform. *Bottom* Schematic representation of histone H3. The K9Me3 residue is pointed by a *black triangle*. In this sequence *brackets* define the sequence region included in the model. Note that residues Arg17 and Lys18 were actually replaced by Gly in the NMR template structure (1GUW) and conserved in this study. **b** Least RMSD fit of the initial (translucent) and final conformers of the HP1β–H3 complex. *Blue* and *yellow* parts of the figure represent HP1β and the H3K9Me3 peptide, respectively. The C carbon of K9Me3 is indicated as a *red ball* for reference. **c** Schematic representation of the interactions discussed in the text. *Red* and *grey dashed lines* indicate Hbond and hydrophobic interactions, respectively. The *red oval* represents a region of negative potential generated by the acidic N-terminal of the Chromodomain. **d** Same as **b**, for the complex with the gamma isoform

corresponds to the first model of the NMR family (best representative conformer in the ensemble of 25 structures).

(ii) A complex of the human HP1γ bound to the same peptide of System *i*. This was obtained by mutating the residues according to the sequence alignment shown in Fig. 1a. Point mutations were introduced removing the side chains of the mutating residues and adding the corresponding atoms in its canonical conformation. Possible clashes were relaxed by global energy minimization (see below).

(iii) A complex of the human HP1β bound to the H3K9Me3 in which *Glu16* and *18* were mutated to *Ala* and *Pro*, respectively. These point mutations were introduced on the final minimized conformer of

system *i* (after 60 ns, see below) following the same procedure used for system *ii*.

(iv) A complex of the human HP1β Chromodomain bound to the H3K9Me3 phosphorylated at Ser10 (H3K9Me3S10p).

(v) Same as *iv* but for the HP1γ isoform. These models were then used as initial coordinates for MD simulations.

Molecular dynamic simulations

All simulations were performed and analysed using the GROMACS 4.0.3 package (van der Spoel et al 2005). The parm99 force field of AMBER with the ff99SB modification

was used to describe standard residues (Wang et al 2000; Hornak et al 2006). The parameters of phosphoserine were taken from (Craft and Legge 2005), while parameterization of trimethyllysine was done in-house following the same protocol used for phosphoserine (Craft and Legge 2005). Counter ions were added to neutralize the system. Solvent was explicitly represented with roughly 7,000 TIP3P water molecules (Jorgensen 1981) in a truncated octahedron box; a concentration of 150 mM of NaCl was added to mimic physiological conditions. The integration time step for the simulations was set to 2.0 fs and all chemical bonds involving Hydrogen atoms were restrained using the Lincs algorithm (Hess et al 1997; Hess 2008). Long-range interactions were treated using the Particle Mesh Ewald approach (Darden et al 1993; Essmann et al 1995) with a 1 nm direct space cut-off. Initially, the whole system was relaxed by performing 1,000 steps of energy minimization. Then, the system was gradually heated from 0 to 300 K during a 500 ps MD run imposing harmonic constraints of $1.0E + 04$ kJ/mol nm^2 to the protein complex and a constant pressure of 1 atm. Final temperature and pressure was reached coupling the system to a Nose–Hoover thermostat (Nosé 1984; Hoover 1985) and a Parrinello–Rahman barostat (Parrinello and Rahman 1981; Nosé and Klein 1983), respectively. System's central of mass motion was linearly removed every 5 ps. Production runs were carried out for 60 ns for systems *i* and *ii*. For system *iii*, production runs were performed for 40 ns from which only the last 30 ns were used for analysis. Since phosphorylation at Ser10 is supposed to further perturb the systems, simulations of phosphorylated systems *iv* and *v* were extended up to 100 ns. System configurations were collected every 1 ps. The last 30 ns of each simulation were used for analysis.

All the dynamic properties reported were calculated using standard utility programs included in the Gromacs 4.0.3 release. Root mean square fluctuations (RMSF) and deviations (RMSD) were calculated on the Cα atoms of each residue.

Difference contacts map was calculated subtracting contact maps averaged over the last 30 ns of the simulations of systems *i* and *ii* as a normal matrix operation.

Electrostatic potentials were calculated using APBS (Baker et al. 2001). Molecular visualization and graphics were performed with VMD (Humphrey et al. 1996).

Distance cut-offs for hydrophobic contacts and salt bridges were set at 0.5 nm. Hydrogen bonds (Hbond) were considered to exist for acceptor–donor distances less than 0.3 nm and the angle acceptor–donor–hydrogen less than 30°.

Binding energies were calculated using an implicit solvation approach to take into account the instantaneous response of solvent dielectric. They were calculated as the difference between the energy of the complex and the sum of the energies of the isolated components along the MD runs. For this aim, we filtered out the trajectories of each complex and its components (water and counterions were striped out). Energies were evaluated within the Generalized Born Model framework as implemented in the sander module of Amber (Tsui and Case 2001). Notice that, strictly speaking, these values rather correspond to binding enthalpies. Furthermore, since energy values are calculated from an effective force field they should be taken as relative indicators of the strength of the interactions in each system and not as absolute values.

Results

Overall description

We used as template the NMR structure of the mouse HP1β Chromodomain in complex with the first 18 residues of H3 (Nielsen et al. 2002). To acquire a comparative overview of the isoform specific and post-transductional modification effects in the HP1–H3 complex we constructed five systems (see Sect. "Methods" for a more detailed description):

(i)   The HP1β Chromodomain bound to the N-terminal 18-mer of H3 trimethylated at Lys9 (H3K9Me3).
(ii) The HP1γ Chromodomain bound to the N-terminal 18-mer of H3K9Me3.
(iii) The HP1β Chromodomain bound to the N-terminal 18-mer of H3K9Me3. In this system, residues *Glu16* and *18* at the Chromodomain were mutated to *Ala* and *Pro*, respectively. This was used as a control to test the involvement of acidic residues at the N-terminal of HP1β on the stability of the complex.
(iv) A complex of the human HP1β Chromodomain bound to the H3K9Me3 phosphorylated at Ser10 (H3K9Me3S10p).
(v)   A complex of the human HP1γ Chromodomain bound to H3K9Me3S10p.

Note that aimed to ease the comparison between both isoforms, the numeration corresponding to the beta isoform is always used in the paper. The right residue numbering of the gamma isoform is shifted by 9 positions to the left (i.e. the first residue in our HP1γ model, which is called Glu15, corresponds actually to Glu24). Furthermore, in order to increase the comprehensiveness of the text, residues belonging to the Chromodomain receptor are hereafter reported in italics, while residues belonging to the H3 peptide are written using normal characters.

All the simulations were characterized by relatively large fluctuations, especially due to the presence of the

highly flexible segments at the N- and C-terminal regions of the H3 peptides. Root mean square deviation (RMSD) calculation for the Chromodomain of HP1β in complex with H3K9Me3 (system i) oscillated around 0.2 nm, which is well compatible with the 0.16 nm measured among the NMR family of structures. Measurement of RMSD for all the other systems studied gave slightly higher values ($\sim$0.3 nm). This could be expected as these systems were obtained as modifications from an experimental structure. Nevertheless, calculation of the cosine content of the first four eigenvectors, which account for more than 60% of the total motion in any of the systems, gave values below 0.4, suggesting a good convergence. The conformation of K9Me3 within the aromatic cage was maintained in all the systems studied. The overall agreement with the experimental data can be also inferred from the global match of the RMSF profiles for all the systems studied when

compared with that obtained from the NMR derived structure (Fig. 2a).

In the following paragraphs we present a comparative view of the results obtained for the different HP1–H3 complexes. Conserved features already described in experimental structures are, in general, omitted.

HP1 isoform-specific interactions with the N-terminal of histone 3

System i: HP1β–H3K9Me3

The HP1β–H3K9Me3 complex reveals the minor modifications from the initial conformation (Fig. 1b). Secondary structure changes were not observed in the Chromodomain neither in the central residues Gln5 to Ser10 flanking K9Me3. This segment keeps a 5-residues long anti-parallel
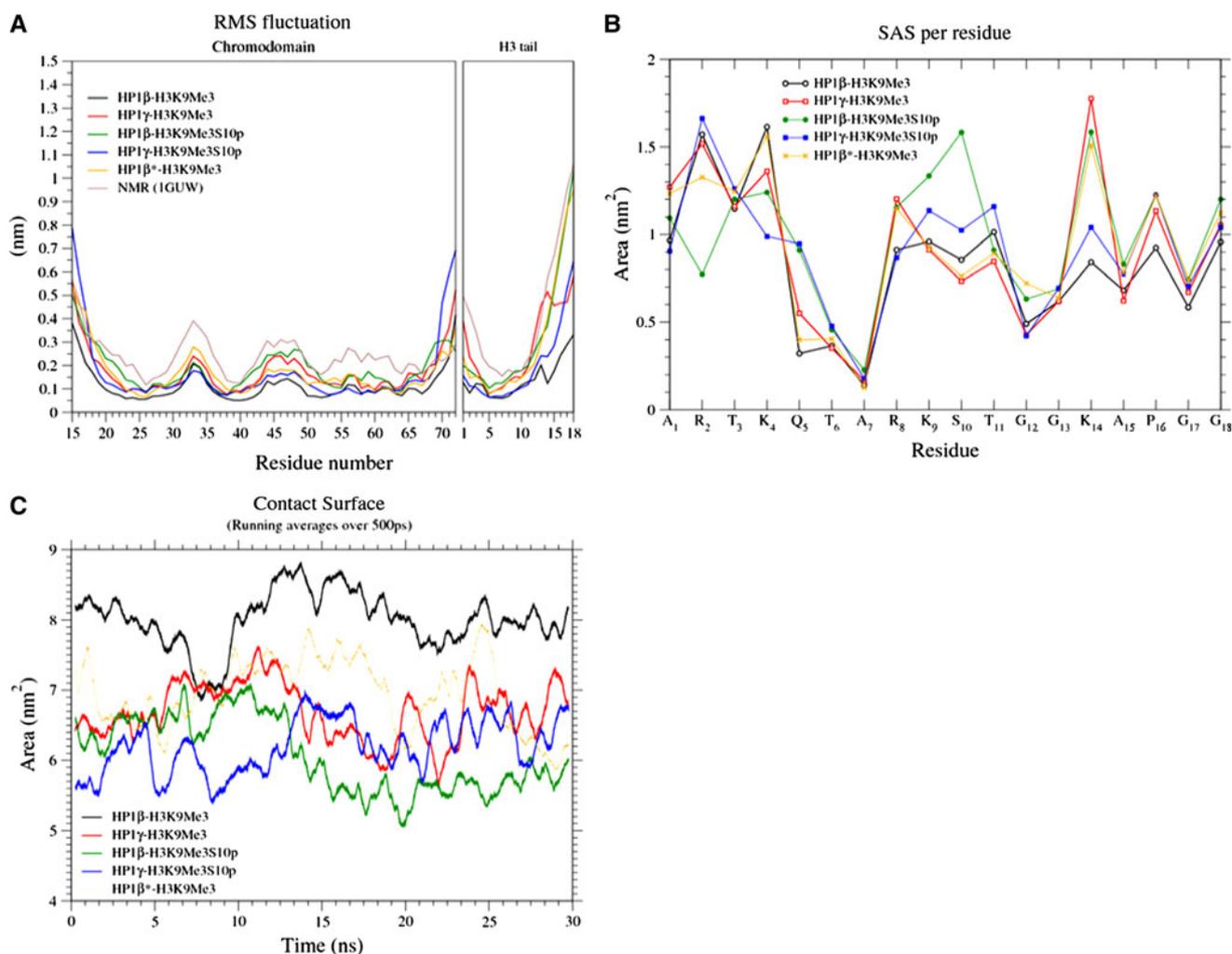

Fig. 2 Comparison of dynamical data extracted from the simulations. **a** RMSF calculated over the Cα atoms. Values for the Chromodomain and H3 peptide are presented on the left and right sides of the figure, respectively. Different systems are indicated by different colours.

HP1β* corresponds to the double mutation, *Glu16Ala*, *Glu18Pro* introduced in HP1β (System *iii*). **b** Solvent accessible surface (SAS) area per residue of the ligand. **c** Instantaneous values of the protein–protein interface area for the MD trajectories

β-sheet conformation (Fig. 1a, b). This interaction is maintained by the formation of several hydrogen bonds between the backbone of the H3-tail and the Chromodomain (Table 1). Molecular dynamics simulation kept the same interactions found in the NMR structure. A global assessment of the fidelity of the MD trajectory when compared with the NMR data can be acquired by comparing the RMSF of the Cα atoms of each residue (Fig. 2a). We obtained a very good qualitative agreement with the peaks corresponding to the N- and C-termini and residues located in loops β1-β2 (residues *Lys33* to *Lys35*), β2-β3 (residues *Lys43* to *Asn50*) and β3-α1 (residues *Glu55* to *Cys60*, see secondary structure assignment in Fig. 1a). In agreement with the experimental data, the low mobility of residues 4 to

10 in the ligand peptide indicates the most stable interactions (Fig. 2a). Inspection of the MD trajectory also allows getting a relative measure of the strength of the interactions (Table 1) and account for the impairing effect of a series of point mutations reported for other Chromodomain/H3 interactions (Jacobs and Khorasanizadeh 2002). In particular, the stringent requirement for a Threonine at position 6 is justified by the simultaneous formation of an Hydrogen bond (Hbond) between its hydroxyl moiety with the carboxyl of *Glu20* and the hydrophobic interaction with the side chains of *Val22* of HP1 Chromodomain (Table 1 and Fig. 1c). The next residue, Ala7 is deeply buried in the protein–protein interface surrounded by the highly conserved *Val23*, *Leu40*, *Trp42* and *Leu58* (Table 1). This tight

Table 1 Comparison of main interactions and binding energies involved in HP1–H3 complexes

| | | HP1β | | | | HP1β$_{E16A,E18P}$ | | HP1γ | | | |
| | | K9Me3 | | K9Me3S10p | | K9Me3 | | K9Me3 | | K9Me3S10p | |
		% Occ	$\tau_{1/2}$	% Occ	$\tau_{1/2}$	% Occ	$\tau_{1/2}$	% Occ	$\tau_{1/2}$	% Occ	$\tau_{1/2}$
Binding energy estimation (kcal/mol)		−106.4		−94.7		−99.3		−94.6		−80.1	
Residue interactions											
	HP1	H3-tail									
Backbone											
HB	Val23:N	Gln5:O	63.1	3	58.6	3	44.3	2	61.5	3	64.6	3
	Asp59:O	Thr6:N	10.6	1	0.0	0	12.8	1	18.7	2	0.0	0
	Asp59:N	Thr6:O	65.3	4	0.0	0	70.2	4	50.3	4	0.0	0
	Tyr[Phe]21:O	Ala7:N	54.3	2	51.2	2	46.6	2	52.7	2	52.3	2
	Tyr[Phe]21:N	Ala7:O	61.3	3	58.9	3	55.7	2	67.4	3	69.0	4
	Asn57:O	Arg8:N	28.9	2	<0.1	1	53.0	3	22.0	2	0.0	0
	Glu19:O	K9Me3:N	0.6	1	61.3	3	49.5	4	3.3	1	0.0	0
Lateral chain											
HB	Asp62:N	Gln5:OE1	18.8	2	0.0	0	18.5	1	30.7	2	0.0	0
	Glu20:OE1(2)	Thr6:OG1	52.5	11	81.9	41	46.4	10	42.5	9	55.9	14
	Glu53:OE1(2)	Ser10:OG	9.4	11	–	–	89.4	22	78.3	43	–	–
	Asn57:ND2	Ser10:OG	10.7	2	0.0	0	0.2	1	1.5	2	0.0	0
SB	Glu20:CD	Arg8:CZ	70.0	14	10.0	5	32.3	12	61.8	9	0.4	2
	Glu19:CD		0.0	0	0.0	0	1.3	5	0.0	0	0.1	1
	Glu18:CD		43.5	3	35.2	15	–	–	–	–	–	–
	Glu17:CD		0.0	0	0.2	6	0.2	7	50.8	12	1.0	18
	Glu16:CD		52.6	24	5.2	4	–	–	–	–	–	–
	Glu15:CD		5.3	11	45.4	12	10.2	10	0.0	0	0.0	0
HC	Val22:CG1(2)	Thr6:CG2	99.0	105	75.5	6	98.9	109	95.5	39	99.9	810
	Val23:CG1(2)	Ala7:CB	99.9	832	99.6	325	99.9	856	79.3	8	97.3	46
	Trp42:CZ3		>99.9	5 ns	>99.9	3.3 ns	100	30 ns	98.9	99	99.9	881
	Trp42:CH2		>99.9	3.3 ns	>99.9	15 ns	>99.9	15 ns	99.0	109	>99.9	5 ns
	Leu40:CD1(2)		98.2	69	99.3	236	98.7	93	39.2	4	42.1	2
	Leu58:CD1(2)		78.3	24	72.1	15	98.8	99	60.8	16	82.9	8

Only interactions between HP1 and the β structured peptide of H3 are reported. Interactions involving K9Me3, which are conserved in all the simulations, are not included for the sake of brevity. The occurrence time (% Occ) was calculated as the percentage of time on which the interaction is observed over the last 30 ns of each trajectory. The average lifetime ($\tau_{1/2}$) of the interactions are reported in pico seconds (ps) unless ns (nano second) is indicated

HB hydrogen bonds, *HC* hydrophobic contacts, *SB* salt bridges

hydrophobic coordination combined with the reduced size of the hydrophobic cavity clearly explains the drastic reduction of an Ala7Met replacement (Jacobs and Khorasanizadeh 2002). Proceeding on the H3 sequence we found Arg8, the mutation of which into Alanine reduces Chromodomain binding by nearly two orders of magnitude (Jacobs and Khorasanizadeh 2002). In fact, this basic residue occupies a key position to interact with *Glu16, 18* and *20* (Table 1, Fig. 1c). Then, K9Me3, the trimethyl ammonium moiety of which remains tightly coordinated by the triple aromatic cage formed by *Tyr21*, *Trp42* and *Tyr45* along the whole simulation. Subsequently, Ser10, which is target of phosphorylation, establish in this isoform only transient electrostatic interactions with *Glu53* and *Asn57*, probably due to solvent competition. This furnishes a putative explanation for the mild affinity loss upon mutation into Alanine (Jacobs and Khorasanizadeh 2002). Another interesting residue is Lys14, which is target of acetylation (Yang 2004). In close similarity with Ser10, post-transductional modification at Lys14 has been proposed to mediate dissociation (Mateescu et al. 2004). A supposed explanation for this effect could be the neighbourhood of the amide moiety of Lys14 with the negative region generated by the six consecutive Glutamate residues at the N-terminal of the HP1β Chromodomain (Fig. 1c). However, these contacts are not stiffly maintained during the simulation, suggesting a rather unspecific interaction. It is, hence, possible that turning off the positive charge by acetylation may decrease the binding affinity by reducing the global coulombic attraction.

System ii: HP1γ–H3K9Me3

The simulation of the HP1γ isoform did not show dramatic changes in the global structure of the complex with respect to HP1β (Fig. 1b, d). The main structural distortion resides in the loss of the last helical turn, although it does not seem to have a direct effect in the intermolecular interactions. The anti-parallel β-sheet conformation in the core of the H3 peptide is kept within the binding site. Indeed, Hbond interactions involved in the central β-sheet remain essentially unchanged (Table 1). However, the lack of electrostatic interactions originated by the substitution of *Glu16* and *18* in HP1β for *Ala16* and *Pro18* in HP1γ generate some structural instability that translate in a slightly lower affinity. Calculation of the average binding energy during the trajectory showed a decrease of nearly 10% (Table 1). This is consistent with the behaviour of protein–protein interface area, which in HP1γ evolves to lower values with respect to the beta isoform (Fig. 2c). In line with this, the number of salt bridge interactions engaged by Arg8 is reduced (Table 1). Additionally, we observe an almost complete loss of interactions between the N-terminal

region of the Chromodomain and Lys14. This situation can also be inferred from the increase in the solvent accessible surface of both residues as compared with the HP1β complex (Fig. 2b).

Absence of electrostatic stabilization translates in a higher flexibility (Fig. 2a). The largest differences in RMSF between both Chromodomain variants are observed in the region belonging to the loop β2-β3, which contains *Phe45*, one of the three aromatic residues involved in the cation-π interaction with K9Me3. Furthermore, a large rise in RMSF is observed on the C-terminal half of the peptide that moves freely without establishing any stiff interaction during the simulated time window (Fig. 2a).

A comparative overview of the dissimilarities concerning both isoforms can be acquired by inspection of the different contact maps averaged over the trajectory (Fig. 3). The diagonal elements of the symmetric map represent self-residue contacts, which are obviously always present and conserved. Off-diagonal elements are indicative of diverse inter-residue contacts along the trajectory of both isoforms. In this representation, green pixels (background) correspond to the zero in the scale and represents contacts conserved in both isoforms. Colours to the left in
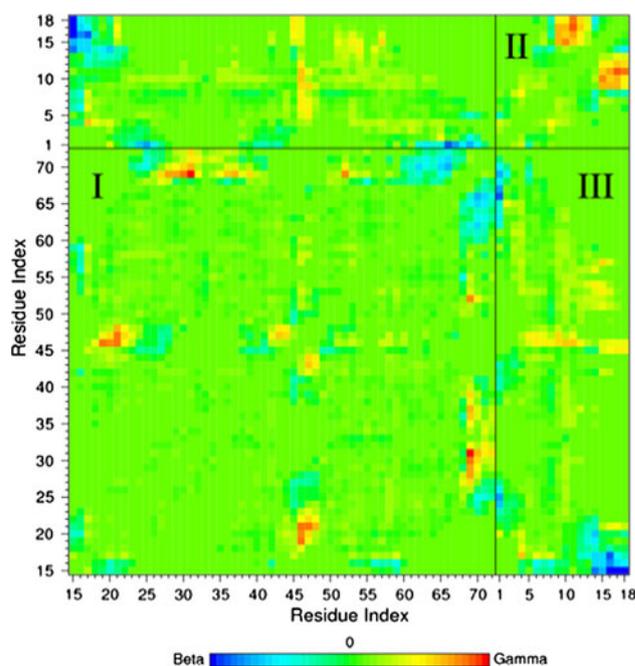

Fig. 3 Difference contact map. This map was obtained as the matrix difference between the contact map averaged over the last 30 ns of the trajectories of systems *i* and *ii*. The map is symmetric with respect to the positive diagonal. Each pixel corresponds to a single amino acid. *Green pixels* indicate contacts conserved in both simulations. The colour scale runs according to the light spectrum, where *blued pixels* are indicative of contacts observed only in the beta isoform and *yellow* or *reddish pixels* are observed only in the gamma isoform. Regions I, II and III contains intra-Chromodomain, intra-peptide and Chromodomain–peptide interactions, respectively

the scale (blued pixels) are indicative of inter-residue contacts present only in the HP1β. Yellow or reddish regions indicate contacts present solely in HP1γ (Fig. 3). The blued (reddish) the colour, the longer the occurrence of the inter-residue contacts during the simulation.

Inspection of the intra-Chromodomain interactions (region I in Fig. 3) indicate that only minor variations are observed going from one isoform to the other and these are due to sequence dissimilarities (see also Fig. 1a). The more evident contact variations within the Chromodomains regard the C-terminal of the protein (residues *Leu68* to *Lys72*). These regions interact preferentially with nearby amino acids *Glu62* to *Phe67* in HP1β while the same segment is in touch with residues *Leu27* to *Phe39* in HP1γ. This is due to the loss of secondary structure in that region (Fig. 1d) originating a more flexible C-terminal segment that is able to sample a wider conformational space. Furthermore, residues *Thr46* to *Ala48* interact with *Glu19* to *Val22* and *Trp42* to *Gly44* only in HP1γ.

The region of the map covering the intra-peptide interaction (region II in Fig. 3) reveals contacts between the middle-terminal segments of the ligand in HP1γ. These contacts are not present in HP1β due to the more stable interaction with Lys14, which anchors the C-terminal of the peptide.

Examination of the region III, corresponding to the Chromodomain–peptide, shows that due to the more rigid conformation of the peptide, the N- and C-termini of the HP1β Chromodomain engage stable interactions with the C- and N-termini of the ligand, respectively. Conversely, the disordered behaviour of the ligand in complex with HP1γ results in more spread contacting regions.

System iii: probing the role of isoform-specific electrostatic interactions

Comparative analysis of the simulations of systems *i* and *ii* points to a fundamental role of charged residues at the N-terminal of the Chromodomain. Aimed to test this hypothesis we constructed a model of an HP1β–H3K9Me3 complex in which we introduced the double mutation *Glu16Ala*, *Glu18Pro* (*System iii*). In this way we can mimic the loss of electrostatic stabilization in HP1γ within the HP1β context. In agreement with our hypothesis, this double mutant recovered the most characteristic features obtained for the HP1γ–H3K9Me3 complex. Not only RMSF shifted to higher values as observed when passing from the beta to the gamma isoform (Fig. 2a), but also the solvent accessible surfaces per residue (Fig. 2b) are strikingly alike to those of the peptide bound to HP1γ. The interaction energy and the complex interface area show intermediate values to those obtained in both isoforms (Table 1 and Fig. 2c). In fact, comparison of the global

electrostatic/hydrophobic interactions reported in Table 1 indicates that this mutant is more similar to HP1γ. This strongly suggests that the isoform-specific differences observed between beta and gamma variants are largely attributable to the *Glu16Ala*, *Glu18Pro* mutations.

Effect of Ser10 phosphorylation

System iv: HP1β in complex with H3K9Me3S10p

Phosphorylation at Ser10 concomitantly with trimethylation at Lys9 in the H3 peptide clearly destabilized the structure of the complex with HP1β. This translates in a lower amount of Hbond interactions (Table 1). In particular, the anti-parallel β-sheet is shortened in H3 with respect to both non-phosphorylated forms, although there is a partial compensation due to the creation of a new Hbond between the backbone amide group of K9Me3 and *Glu20* (Table 1). Still, due to the augmented flexibility of the N- and C-termini of the peptide, the salt bridges between Arg8 and the acidic N-terminal of the Chromodomain are sensibly reduced as well as the rest of the Hbond interactions listed in Table 1. The reason for this behaviour is that upon post-transductional modification, S10p increases significantly its solvent accessible surface. This slightly pulls out K9Me3, which increments its solvent accessible surface (Fig. 2b). Additionally, the separation of S10p drives the disruption of the electrostatic interactions established by Lys14 raising the solvent exposure of this residue as found in systems *ii* and *iii* (Fig. 2b).

Calculation of the protein–protein interface indicates a significant reduction upon phosphorylation (Fig. 2c), resulting even lower than the interface area measured for HP1γ. Nevertheless, we were not able to identify a clear indicator of complex dissociation within the time scale explored. Indeed, the hydrophobic interactions established by Ala7, which is deeply buried in the protein–protein interface, remain essentially unchanged (Table 1, Fig. 2b). To further investigate this issue, we calculated the back projection of the first 8 eigenvectors on the real space trajectory, which account for more than 70% of the total motion. However, no significant component of the movement was found onto the line determined by the centres of mass of both ligands.

System v: HP1γ in complex with H3K9Me3S10p

Introduction of phosphorylation at Ser10 in HP1γ has similar effects to those described for the beta isoform. Analogously, binding energy decreased nearly a 10% with respect to the unphosphorylated case (Table 1). The anti-parallel β-strand of H3 also shortens by two residues and, in general, all the interactions listed in Table 1 show a similar

variation as observed for the beta isoform. Also in this case no sign of dissociation was evident from the simulation. The main difference with the latter case resides in the interaction of Lys14, which is involved in fleeting electrostatic interactions with *Glu53* and *Asn57*. Similar interactions established between these residues and Ser10 were observed in systems *i* and *ii* (unphosphorylated forms). These interactions result in a smaller decrease in the protein–protein interface area when compared with system *iv* (Fig. 2c).

Discussion and conclusions

Transcription of the integrated HIV-1 provirus is ruled by chromatin organization, host cell transcription factors and chromatin modifying complexes that may promote the formation of a latent viral reservoir. The latent HIV-1 proviral 5′ LTR is organized into a defined structure composed by two positioned nucleosomes flanking the enhancer region. Besides the non-acetylated state of these LTR-associated nucleosomes, they further suffer H3 trimethylation at Lys9, which cause transcriptional silencing upon the recruitment of HP1 (Sadowski et al. 2008). It has been pointed that the gamma isoform of HP1 is a main determinant of the chromatin-mediated HIV-1 transcriptional silencing and post-integration latency (du Chéné et al. 2007). More recent evidence has suggested a kind of switching mechanism in which HP1β is replaced by the HP1γ isoform (Mateescu et al. 2008). In this context, the structural characterization of the isoform-specific interactions that define the binding preference for the trimethylated H3 tail is very important for a better understanding of the processes that rule the epigenetic control and for the rational design of small molecules able to selectively disrupt such protein–protein interactions. Aimed to provide structural insights into these interactions we have presented here a series of molecular simulations of the HP1 Chromodomain (isoforms beta and gamma) in complex with the N-terminal tail of H3 performed under homogeneous conditions. We also investigated the role of H3 phosphorylation at Ser10 since this modification has been proposed to mediate HP1–H3 dissociation (Fischle et al. 2005; Hirota et al. 2005; Johansen and Johansen 2006).

Sequence alignment of the three human HP1 isoforms indicates overall high identity conservation, especially in the structured domains (Fig. 1a). Although binding is mainly determined by the cation-π interaction, it is expected that isoform-specific interactions may modulate the molecular recognition. In qualitative agreement with experimental reports, we found better stabilization energy for the beta isoform adduct (Fischle et al. 2005). Our results underline the relevance of non-conserved residues at the N-terminal of the HP1 Chromodomain for the H3

binding although they are not expected to have any structural consequence for the structure of the isolated Chromodomains. Notably, these residues interact with Lys14 at H3, which is target of acetylation. This electrostatic interaction results very important for the stability of the bound peptide, which remains in a more extended and stable conformation in the complex with HP1β, while it results more flexible in the HP1γ adduct. This interaction seems to account for most of the isoform-specific effects since a very similar binding pattern is retrieved by introducing the two *Glu16Ala*, *Glu18Pro* mutations in the HP1β Chromodomain. The specificity of these effects is highlighted by the fact that these modifications are present only in the gamma isoform, while Glutamate residues are conserved in the alpha and beta variants (Fig. 1a).

Introduction of phosphorylation at Ser10 translate into a putatively less stable interaction in both isoform complexes. This can be seen from a higher mobility of the peptide segments at N- and C-terminal of K9Me3, which remain stably bound to the aromatic cage. Although we observed a reduction in the Hbond interactions that anchor the H3 β-strand to the binding site, a reduced binding energy, a slight increase in the solvent accessible surface of the binding peptide and a reduction of the protein–protein interface area, the ligands remained bound without an evident tendency to dissociation. In line with this observation, several experimental studies indicate that S10p may not be enough for dissociation to happen (Mateescu et al. 2004). It has also been suggested that concomitant acetylation at Lys14 is needed to detach H3 from HP1 (Mateescu et al. 2004). If this were the case, our results would suggest that the lack of interactions between Lys14 and the acidic residues at the N-terminal could be part of the release mechanism. Furthermore, it could be conjectured that this modification might be less effective in the context of the gamma isoform, where Ser10 phosphorylation could be better tolerated. This can be inferred from the electrostatic potential to which the binding peptides are exposed by the receptor. As illustrated in Fig. 4, the electrostatic potential generated by the HP1β isoform is more negative, especially in the region surrounding Ser10.

Of course, we have to keep in mind some intrinsic limitations of the theoretical methods, such as the limited sampling time, absence of polarization effects, rough description of cation-π interaction, etc. We also have to underline that a strong bias is imposed in the simulations of phosphorylated systems by assuming that the doubly modified peptides are bound to the Chromodomain. Another, perhaps the more important, shortcut regards the suboptimal reproduction of interactions arising from the lack of biological environment whose effects are impossible to estimate. Nevertheless, state of the art simulations as those presented in this contribution performed under homogeneous conditions may help to pin
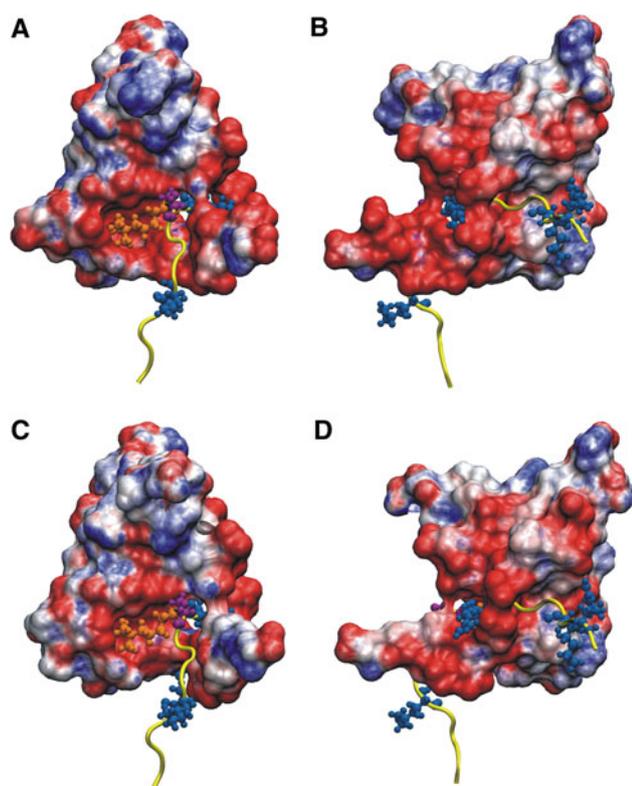
Fig. 4 Electrostatic potential mapped on the HP1 solvent accessible surfaces (Connolly type surface, Varshney et al 1994). The electrostatic potential was calculated only for the Chromodomain receptors previous to each MD to allow for a better comparison. Molecular representations of the ligand are included in the figure but they were not used in the calculation. *Red*, *white* and *blue* regions correspond to negative, neutral and positive potential, respectively. K9Me3 residue is coloured in *orange*, while Ser10 and all the basic residues present in the H3 peptide (Arg2, 8 and Lys4, 14) are coloured in *purple* and *blue*, respectively. **a** and **b** Electrostatic potential for HP1β rotated 180° around the vertical axis. **c** and **d** same as **a** and **b** for HP1γ

down isoform-specific interactions that define the binding preference for a given target. In particular, the absence of acidic residues at the N-terminal segment of HP1γ may be exploited as a selectivity determinant for the rational design of small molecules able to selectively disrupt these protein–protein interactions.

References

Baker NA, Sept D, Joseph S, Holst MJ, McCammon JA (2001) Electrostatics of nanosystems: application to microtubules and the ribosome. Proc Natl Acad Sci USA 98:10037–10041

Ball LJ, Murzina NV, Broadhurst RW, Raine AR, Archer SJ, Stott FJ, Murzin AG, Singh PB, Domaille PJ, Laue ED (1997) Structure of the chromatin binding (chromo) domain from mouse modifier protein 1. EMBO J 16:2473–2481

Bannister AJ, Zegerman P, Partridge JF, Miska EA, Thomas JO, Allshire RC, Kouzarides T (2001) Selective recognition of methylated lysine 9 on histone H3 by the HP1 chromo domain. Nature 410:120–124

Clavel F, Hance AJ (2004) HIV drug resistance. N Engl J Med 350:1023–1035

Craft JW, Legge GB (2005) An AMBER/DYANA/MOLMOL phosphorylated amino acid library set and incorporation into NMR structure calculations. J Biomol NMR 33:15–24

Darden T, York D, Pedersen L (1993) Particle Mesh Ewald: an Nlog(N) method for Ewald sums in large systems. J Chem Phys 98:10089–10092

du Chéné I, Basyuk E, Lin YL, Triboulet R, Knezevich A, Chable-Bessia C, Mettling C, Baillat V, Reynes J, Corbeau P, Bertrand E, Marcello A, Emiliani S, Kiernan R, Benkirane M (2007) Suv39H1 and HP1gamma are responsible for chromatin-mediated HIV-1 transcriptional silencing and post-integration latency. EMBO J 26:424–435

Essmann U, Perera L, Berkowitz ML, Darden T, Lee H, Pedersen LG (1995) A smooth particle mesh Ewald method. J Chem Phys 103:8577–8593

Fischle W, Tseng BS, Dormann HL, Ueberheide BM, Garcia BA, Shabanowitz J, Hunt DF, Funabiki H, Allis CD (2005) Regulation of HP1-chromatin binding by histone H3 methylation and phosphorylation. Nature 438:1116–1122

Grewal SI, Moazed D (2003) Heterochromatin and epigenetic control of gene expression. Science 301:798–802

Hess B (2008) P-LINCS: a parallel linear constraint solver for molecular simulation. J Chem Theory Comput 4:116–122

Hess B, Bekker H, Berendsen HJC, Fraaije JGEM (1997) LINCS: a linear constraint solver for molecular simulations. J Comput Chem 18:1463–1472

Hirota T, Lipp JJ, Toh BH, Peters JM (2005) Histone H3 serine 10 phosphorylation by Aurora B causes HP1 dissociation from heterochromatin. Nature 438:1176–1180

Hoover WG (1985) Canonical dynamics: equilibrium phase-space distributions. Phys Rev A 31:1695–1697

Hornak V, Abel R, Okur A, Strockbine B, Roitberg A, Simmerling C (2006) Comparison of multiple amber force fields and development of improved protein backbone parameters. Proteins 65:712–725

Humphrey W, Dalke A, Schulten K (1996) VMD: visual molecular dynamics. J Mol Graph 14:33–38

Jacobs SA, Khorasanizadeh S (2002) Structure of HP1 chromodomain bound to a lysine 9-methylated histone H3 tail. Science 295:2080–2083

Jacobs SA, Taverna SD, Zhang Y, Briggs SD, Li J, Eissenberg JC, Allis CD, Khorasanizadeh S (2001) Specificity of the HP1 chromo domain for the methylated N-terminus of histone H3. EMBO J 20:5232–5241

Johansen KM, Johansen J (2006) Regulation of chromatin structure by histone H3S10 phosphorylation. Chromosome Res 14:393–404

Jorgensen WL (1981) Transferable intermolecular potential functions for water, alcohols, and ethers. Application to liquid water. J Am Chem Soc 103:335–340

Lachner M, O'Carroll D, Rea S, Mechtler K, Jenuwein T (2001) Methylation of histone H3 lysine 9 creates a binding site for HP1 proteins. Nature 410:116–120

Lehrman G, Hogue IB, Palmer S, Jennings C, Spina CA, Wiegand A, Landay AL, Coombs RW, Richman DD, Mellors JW, Coffin JM, Bosch RJ, Margolis DM (2005) Depletion of latent HIV-1 infection in vivo: a proof-of-concept study. Lancet 366:549–555

Maison C, Almouzni G (2004) HP1 and the dynamics of heterochromatin maintenance. Nat Rev Mol Cell Biol 5:296–304

Marban C, Suzanne S, Dequiedt F, de Walque S, Redel L, Van Lint C, Aunis D, Rohr O (2007) Recruitment of chromatin-modifying enzymes by CTIP2 promotes HIV-1 transcriptional silencing. EMBO J 26:412–423

Martinez-Cajas JL, Wainberg MA (2008) Antiretroviral therapy: optimal sequencing of therapy to avoid resistance. Drugs 68:43–72

Mateescu B, England P, Halgand F, Yaniv M, Muchardt C (2004) Tethering of HP1 proteins to chromatin is relieved by phospho-acetylation of histone H3. EMBO Rep 5:490–496

Mateescu B, Bourachot B, Rachez C, Ogryzko V, Muchardt C (2008) Regulation of an inducible promoter by an HP1beta-HP1gamma switch. EMBO Rep 9:267–272

McKinnon JE, Mellors JW, Swindells S (2009) Simplification strategies to reduce antiretroviral drug exposure: progress and prospects. Antivir Ther 14:1–12

Minc E, Courvalin JC, Buendia B (2000) HP1gamma associates with euchromatin and heterochromatin in mammalian nuclei and chromosomes. Cytogenet Cell Genet 90:279–284

Nielsen AL, Oulad-Abdelghani M, Ortiz JA, Remboutsika E, Chambon P, Losson R (2001) Heterochromatin formation in mammalian cells: interaction between histones and HP1 proteins. Mol Cell 7:729–739

Nielsen PR, Nietlispach D, Mott HR, Callaghan J, Bannister A, Kouzarides T, Murzin AG, Murzina NV, Laue ED (2002) Structure of the HP1 chromodomain bound to histone H3 methylated at lysine 9. Nature 416:103–107

Nosé S (1984) A molecular dynamics method for simulations in the canonical ensemble. Mol Phys 52:255–268

Nosé S, Klein ML (1983) Constant pressure molecular dynamics for molecular systems. Mol Phys 50:1055–1076

Parrinello M, Rahman A (1981) Polymorphic transitions in single crystals: a new molecular dynamics method. J Appl Phys 52:7182–7190

Pierson T, McArthur J, Siliciano RF (2000) Reservoirs for HIV-1: mechanisms for viral persistence in the presence of antiviral immune responses and antiretroviral therapy. Annu Rev Immunol 18:665–708

Sadowski I, Lourenco P, Malcolm T (2008) Factors controlling chromatin organization and nucleosome positioning for establishment and maintenance of HIV latency. Curr HIV Res 6:286–295

Tsui V, Case DA (2001) Theory and applications of the generalized Born solvation model in macromolecular simulations. Biopolymers 56:275–291

van der Spoel D, Lindahl E, Hess B, Groenhof G, Mark AE, Berendsen HJC (2005) GROMACS: fast, flexible and free. J Comp Chem 26:1701–1718

Varshney A, Brooks FP, Wright WV (1994) Computing smooth molecular surfaces. IEEE Comput Graph Appl 14:19–25

Wang J, Cieplak P, Kollman PA (2000) How well does a restrained electrostatic potential (RESP) model perform in calculating conformational energies of organic and biological molecules? J Comput Chem 21:1049–1074

Yang XJ (2004) Lysine acetylation and the bromodomain: a new partnership for signaling. Bioessays 26:1076–1087

Ylisastigui L, Archin NM, Lehrman G, Bosch RJ, Margolis DM (2004) Coaxing HIV-1 from resting CD4 T cells: histone deacetylase inhibition allows latent viral expression. AIDS 18:1101–1108